Environmental Earth Sciences (2022) 81:221
https://doi.org/10.1007/s12665-022-10339-3

ORIGINAL ARTICLE

Rapid ground subsidence in the Küçük Menderes Graben (W. Turkey) captured by Sentinel-1 SAR data

Mumin Imamoglu[1,2] · **Fusun Balik Sanli**[2] · **Ziyadin Cakir**[3] · **Fatih Kahraman**[4]

Received: 27 May 2021 / Accepted: 9 March 2022

Abstract

Over the past few decades, surface deformations have been observed and measured geodetically at many places all over the world, including Central and western Turkey. Surface deformations in some of these regions have been attributed to aseismic slip-on faults and/or to excessive pumping of groundwater. In this study, we present our investigation on the ground subsidence in Ödemiş town (W. Turkey) located in the Küçük (K.) Menderes Graben where one of the most severe and widespread surface fracturings has been reported. The entire graben is analyzed using the Sentinel-1 synthetic aperture radar (SAR) data with multi-temporal interferometric SAR techniques. A total of 342 single look complex products acquired in 2015–2018 are processed using the Small Baseline Subset method. Vertical mean velocity fields reveal that K. Menderes Graben is experiencing extensive subsidence at rates reaching as much as 29 cm/year, making it one of the fastest subsiding regions in the world. The spatial correlation between the subsiding regions and the unconsolidated sediments suggests that the subsidence is most probably due to over drafting of the groundwater, which is confirmed by the strong temporal correlation between displacement time series and groundwater level changes. Inelastic/elastic deformation ratios calculated for the entire graben suggest that inelastic deformation is the dominant component in the region, implying an irreversible deformation. Skeletal storage coefficients calculated at well locations also support the idea of inelastic deformation. However, severe inelasticity is not extensive, and the region may still recover from subsidence with correct groundwater management.

Keywords InSAR time series · Sentinel-1 · Land subsidence · Küçük Menderes Graben · Western Turkey

Introduction

Ground deformation caused by natural or human-induced activities is a common geological phenomenon which is observed all over the world (Herrera-García et al. 2021). It may occur as a result of natural mechanisms, such as tectonic movements and volcanic eruptions, or human-induced activities, such as mining, natural gas and oil extraction, tunnel construction, and in particular, excessive pumping of groundwater. To minimize and mitigate the potential hazard that may be caused by ground deformations, it is necessary to have an effective monitoring system.

There are various ground deformation monitoring techniques that make use of geodetic techniques, such as GPS, leveling and InSAR. Although conventional approaches, such as GPS and leveling, provide highly accurate measurements at mm scale, they could only be used in pre-specified locations or very small areas (Besoya et al. 2021). Moreover, these techniques are both costly, time-consuming and mostly require field investigations. Whereas, InSAR is a powerful

✉ Mumin Imamoglu
mumin.imamoglu@tubitak.gov.tr

Fusun Balik Sanli
fbalik@yildiz.edu.tr

Ziyadin Cakir
ziyadin.cakir@itu.edu.tr

Fatih Kahraman
fatih.kahraman@eng.bau.edu.tr

1 Informatics and Information Security Research Center, TUBITAK, 41470 Gebze, Turkey

2 Department of Geomatic Engineering, Civil Engineering Faculty, Yildiz Technical University, 34220 Istanbul, Turkey

3 Department of Geological Engineering, Istanbul Technical University, 34469 Istanbul, Turkey

4 Applied Artificial Intelligence Center, Faculty of Engineering, Bahçeşehir University, Istanbul, Turkey

Published online: 01 April 2022

remote sensing technique that can cover large areas (up to 400 km) with a high spatial resolution (5–15 m) and high accuracy (sub cm). With the development of new generation radar satellites, such as TanDEM-X, CosmoSkyMed, ALOS-2 and Sentinel-1, the InSAR technique in a way has become a standard technique for earth deformation monitoring in the last decade (Biggs and Wright 2020). It has been widely used for monitoring mining activities (Yang et al. 2020; Fan et al. 2021), subway construction (Xu et al. 2020; Gheorghe et al. 2020; Fadhillah et al. 2020; Halicioglu et al. 2021) structural stability (Lanari et al. 2020b; Selvakumaran 2020; D'Amico et al. 2020), oil production (Chang et al. 2019; Staniewicz et al. 2020), tectonic movements (Elliott et al. 2020; Weiss et al. 2020; Bletery et al. 2020) and landslides (Bekaert et al. 2020; Aslan et al. 2020; Solari et al. 2020). Free-of-charge availability, ease of distribution, and wide spatial coverage (250 km wide) of Sentinel-1 images and cloud computing have made the InSAR technique for nationwide (De Luca et al. 2017; Kalia et al. 2017; Gee et al. 2019; Dehls et al. 2019; Emil et al. 2021) and even continent-wide deformation monitoring possible (Lanari et al. 2020a; Crosetto et al. 2020)

In Western Turkey, surface deformations like fractures, fissures and vertical dislocations at the Earth's surfaces that resemble normal faulting have been observed in the last 10–20 years (Demirtaş et al. 2021). Bolvadin, Sarıgöl, Ödemiş, Kınık, Bursa and Söke are just a few of the districts where these surface deformations have been observed so far. The Gediz Graben in which Sarıgöl is located has been previously analyzed by Poyraz and Hastaoğlu (2020) who claim that surface deformations are due to not only seasonal underground water level changes, but also tectonic movements. While it is emphasized by Imamoglu et al. (2019) that observed surface deformations in Bolvadin and its surroundings in Afyon-Akşehir Graben occur only as a result of excessive use of groundwater, it is thought by Ozkaymak et al. (2019) that the active fault lines in the region may also have an effect on these deformations. The subsidence in the Bursa Plain is mainly related to anthropogenic activities in the region (Aslan et al. 2019). Three different regions around Ödemiş settlement are reported to have long and wide surface deformations mainly as a result of excessive use of groundwater (Demirtaş et al. 2002).

Many studies have been conducted on various subjects about the K. Menderes Basin. Spatio-temporal drought analysis (Eris et al. 2020), irrigation water management (Pusatli et al. 2009), recharge potential of the aquifer (Sayit and Yazicigil 2012), impacts of climate change on groundwater recharge (Yagbasan 2016), erosion risk areas (Gülersoy and Çelik 2015), the structural formation of the graben (Rojay et al. 2005) are some examples of different studies about the K. Menderes Basin. However, no subsidence analysis of the entire region has been reported. Therefore, in this study, our aim is to overcome the lack of subsidence analysis in K. Menderes Graben and its probable causes. To analyze the subsidence phenomenon in K. Menderes Graben, the Sentinel-1 data acquired between 2015 and 2018 inclusive and the advanced InSAR techniques have been used. Advanced multi-temporal InSAR techniques include two main approaches called Persistent Scatterer Interferometry (PSI) and Small Baseline Subset (SBAS). PSI techniques exploit persistent scatterer properties of earth surface and are mostly used for subsidence analysis in urban areas. On the contrary, SBAS methods are developed to analyze distributed scatterers on the earth's surface and are more suitable for deformation analysis of rural areas. In this study, the SBAS approach is selected as multi-temporal InSAR analysis since K. Menders Graben mostly contains a rural environment.

Study area

K. Menderes Graben is located in Western Turkey between Gediz (north and east) and Büyük Menderes (south) basins as shown in Fig. 1. Küçük Menderes River, from which the basin is named, is the most important river in the region. It is surrounded by Bozdağlar Mountains in the north and Aydın Mountains in the south. A flat graben, again named K. Menderes, was formed in the east-west direction with alluvial deposits carried along the K. Menderes River and its tributaries coming from the steep mountains around it (Rojay et al. 2005). It is part of the Western Anatolian Graben family (Dumont et al. 1979).

Küçük Menderes Basin has fertile soils and high agricultural potential in terms of both product quality and yield. Major agricultural products are olive, cotton, wheat, potatoes, and tobacco (Izmir 2019). According to CORINE Land Cover (CLC) maps produced in 2018, Fig. 2, permanently irrigated lands form a large part of the agricultural areas. Groundwater is the main irrigation source of the region. 92.7% of irrigation in 2016 has been reported to be carried out by groundwater (Şahin et al. 2018). In addition to irrigation, groundwater is extracted also for industry and in house use. However, 78% of the total amount of groundwater drawn is used for agriculture purposes (Izmir 2019). The drastic drop in groundwater level observed before 2012 was attributed by (Sayit and Yazicigil 2012) to the excessive use of groundwater for irrigation. Observations at groundwater wells reveal the decline of groundwater level throughout the whole basin (Şahin et al. 2018; TOB 2018).

The seismicity of the region between 1990 and 2019 is shown together with its magnitudes and frequencies in Fig. 1 (KOERI 2021). The active fault database of Turkey is renewed by the Geological Research Department of the General Directorate of Mineral Research and Exploration (MTA)

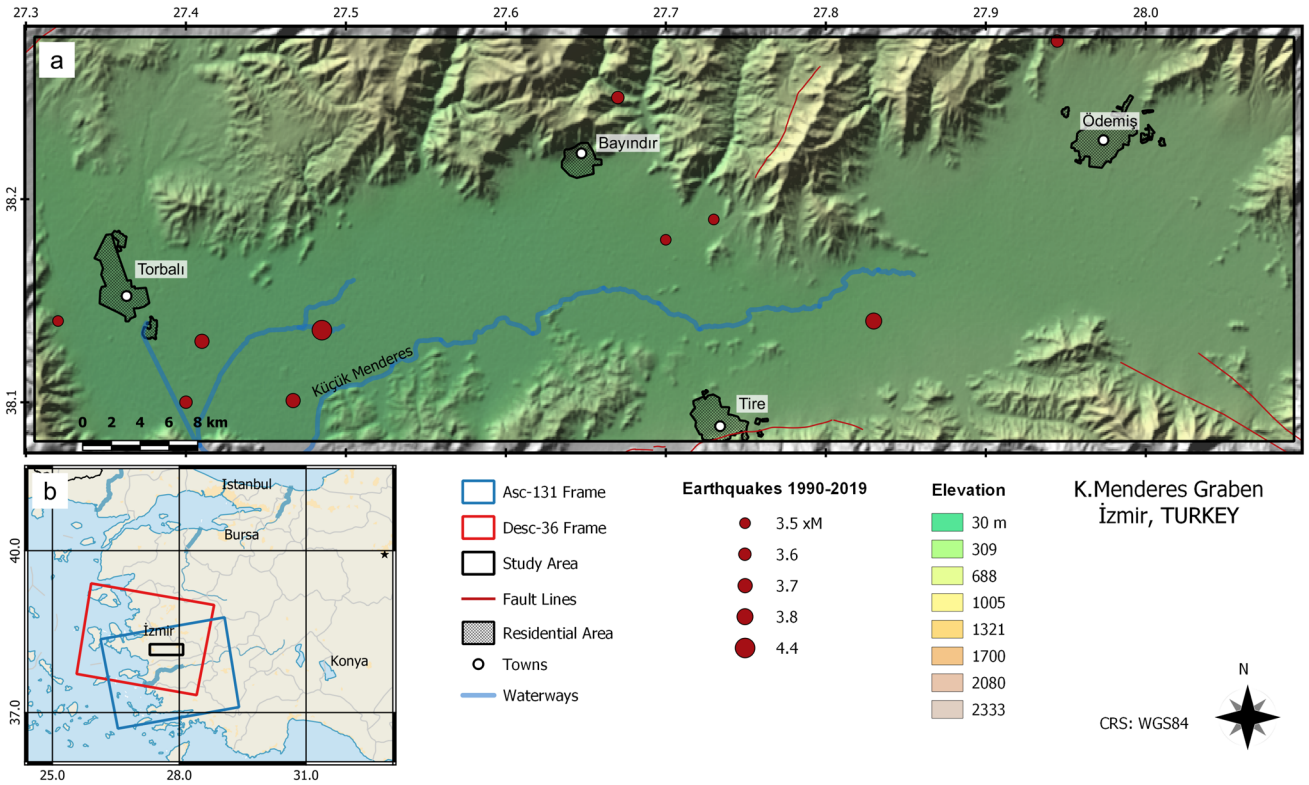

Fig. 1 Location of the study area, K. Menderes sub-basin (Western Turkey) and **a** surroundings with shaded topography, active faults and seismicity between 1990 and 2019 and **b** Sentinel-1 frames used in analysis

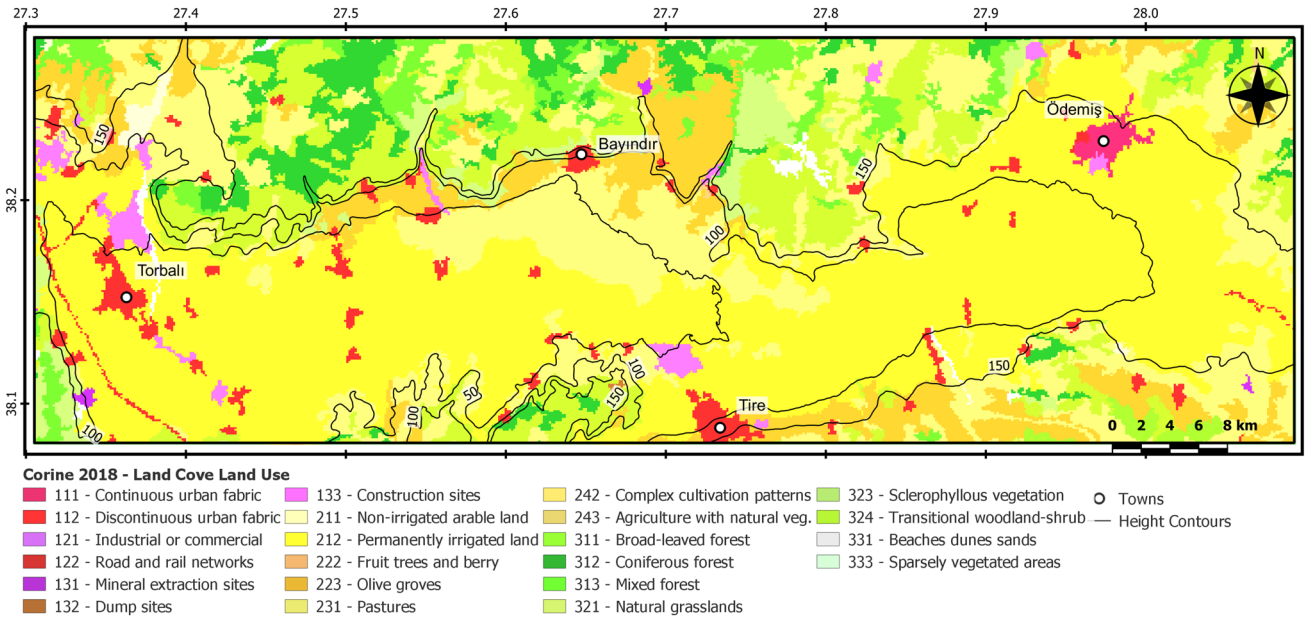

Fig. 2 CORINE Land Cover 2018 maps of study area. Permanently irrigated lands are indicated with label 212 and yellow colour cover very large areas throughout the region

of Turkey (Emre et al. 2018). Active faults of Western Anatolia in Fig. 1 were obtained from the renewed active fault map. Although Western Turkey is a highly active region in terms of tectonics, K. Menderes Graben does seem to be less

affected by these earthquakes since there are no active fault systems within its close vicinity. Ground deformation analysis in the presence of active faults in the region requires a detailed mapping of active faults and their kinematics, similar to those in Afyon-Akşehir and Gediz Graben (Imamoglu et al. 2019; Poyraz and Hastaoğlu 2020).

Materials and methods

SAR dataset

Sentinel-1 is a twin satellite constellation of the European Space Agency (ESA) that provides SAR data free of charge under the Copernicus program. Sentinel-1 A, launched on 3 April 2014, and Sentinel-1 B, launched on 25 April 2016, operate on the same orbital plane and offer a 6-day repeat cycle. It has a C-band (~5.6 cm wavelength) sensor payload which ensures continuity of ERS-1/2 and ENVISAT ASAR satellites with higher temporal resolution and wider coverage. One of the design missions of Sentinel-1 is to facilitate the formation of SAR interferometry for earth observation applications, such as earthquake, glacier, subsidence and landslide monitoring (Torres et al. 2012). The InSAR technique has now become a global monitoring tool over the last decade with the enormous stimulating effect of Sentinel-1, the first satellite mission designed specifically to monitor ground deformation (Biggs and Wright 2020).

While there is only Sentinel-1A data set at the beginning of the analysis period, the temporal resolution increases to 6 days after mid-2016 following the launch of Sentinel-1B. We use Sentinel-1 images acquired in TOPSAR Interferometric Wide (IW) Swath Mode. A total of 342 Sentinel-1 IW images, 167 in ascending and 175 in descending orbit are used for interferogram formation. Table 1 provides detailed information about the Sentinel-1 SAR data used in this study. Temporal and perpendicular baselines of generated interferograms are shown in Fig. 3. The low-quality interferograms shown in red lines were discarded in during the multi-temporal InSAR analysis.

Multi-temporal InSAR processing

Conventional InSAR, where only two SAR images are used to generate a single interferogram, has some limitations and drawbacks for monitoring long-term slow deformation processes (Hanssen and Usai 1997; Klees and Massonnet 1998). Advanced multi-temporal InSAR methods are proposed to overcome the limitations of conventional InSAR, such as temporal decorrelation and atmospheric effects (Hooper et al. 2012; Crosetto et al. 2016; Osmanoğlu et al. 2016; Pepe and Calò 2017). There are two main groups of advanced multi-temporal InSAR techniques that exploit different scattering properties of the earth's surface. In the first approach, called PSI, methods take the advantage of permanent scatterers on the earth surface which show more stable characteristics over a long period without showing any significant sign of temporal decorrelation (Ferretti et al. 2001). Interferograms are formed with respect to a single-reference SAR image within a data set without any spatial/temporal baseline criterion and only persistent scatterer points are analyzed further as measurement points. The second approach, SBAS, aims to decrease temporal decorrelation by enforcing interferogram formation with only small spatial/temporal baselines (Berardino et al. 2002). With the restriction of small baselines, distributed scatterers that could not

Table 1 Sentinel-1 SAR data details

Orbit	Track	Heading angle°	Mean incidence angle°	Products	Interferograms
Ascending	131	350.06	38.99	167	541
Descending	36	191.06	35.98	175	556

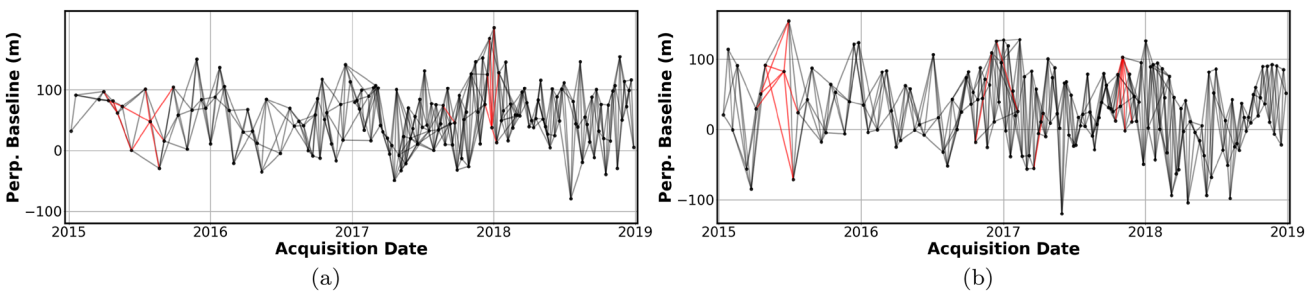

Fig. 3 Perpendicular baselines of interferograms in **a** ascending track 131 and **b** descending track 36. Red lines show unused interferograms with low coherence below the threshold of 0.05

show stable properties over a long period became analyzable. Although more interferograms with the multi-reference images are required, it is possible to obtain more measurement points with that approach, especially in rural environments (Lauknes et al. 2010). While the PSI techniques are the first choice for deformation analysis of urban areas with more permanent scatterers, SBAS methods are mostly preferred for monitoring deformation in rural areas dominant with distributed scatterers (Osmanoğlu et al. 2016).

The K. Menderes Graben is dominated by agricultural areas where temporal decorrelation is inevitable. Therefore, to obtain more measurement points in the study region, the SBAS approach has been chosen as the advanced multi-temporal InSAR analysis method. Unwrapping interferograms and formation of time series are the two main processing categories of the SBAS (Osmanoğlu et al. 2016). The processing steps of these two main categories are carried out with LiCSAR (Lazeckỳ et al. 2020) and LiCSBAS (Morishita et al. 2020) open source tools. LiCSAR is a Sentinel-1 InSAR processor which was developed by the Centre for the Observation and Modelling of Earthquakes, Volcanoes, and Tectonics (COMET). To monitor global tectonic and volcanic zones, Sentinel-1 interferograms are regularly generated and published freely on the COMET-LiCS web portal (LiCSAR 2021). Each Sentinel-1 product is used to generate a total of six interferograms, three with the previous and three with the next adjacent products. Topographic phase components of interferograms are removed using Shuttle Radar Topography Mission (SRTM) (Farr et al. 2007) with 1 arc-second (about 30 m) DEM. All interferograms are processed by Goldstein filter (Goldstein and Werner 1998) and unwrapped with SNAPHU software (Chen and Zebker 2002). Time series InSAR analysis is performed with LiCSBAS open-source software, which is fully compatible with LiCSAR result products. Unwrapped interferograms are downloaded and prepared for time series analysis. Since it is focused on K. Menderes Graben where flat areas are dominant, as in some cases of (Morishita 2021), tropospheric noise correction using the Generic Atmospheric Correction Online Service (GACOS) is not applied. Bad-quality interferograms are identified with a coherence threshold of 0.05 and by checking loop closure. Then, updated unwrapped interferogram stack is inverted to produce displacement time series and velocity maps. In the last step, the results are filtered to decrease the atmospheric noise. The main processing steps of LiCSAR and LiCSBAS tools are summarized in Fig. 4

Vertical and horizontal projection

The InSAR technique can only measure the LOS component of the 3D surface displacement. However, in most applications, it is desired to have three-dimensional (3D) surface displacements in vertical, East–West (E–W), and North–South (N–S) directions. To obtain a 3D displacement, at least three independent acquisition geometries are required (Hu et al. 2014). However, the azimuth direction of polar-orbiting satellites is almost parallel to the N–S direction, as in Sentinel-1. The projection of the N–S component of real displacement onto LOS provides almost no information. However, vertical and E–W components of real 3D displacement can be decomposed from LOS displacements on ascending and descending orbits.

In this study, the method proposed in Hu et al. (2016) is used as the decomposition method to obtain the aforementioned displacement components. Measurement points in ascending and descending data sets might not be the same for all locations. While some locations could provide sufficient coherency in one acquisition geometry, they may not in another acquisition geometry. Therefore, when coherency is

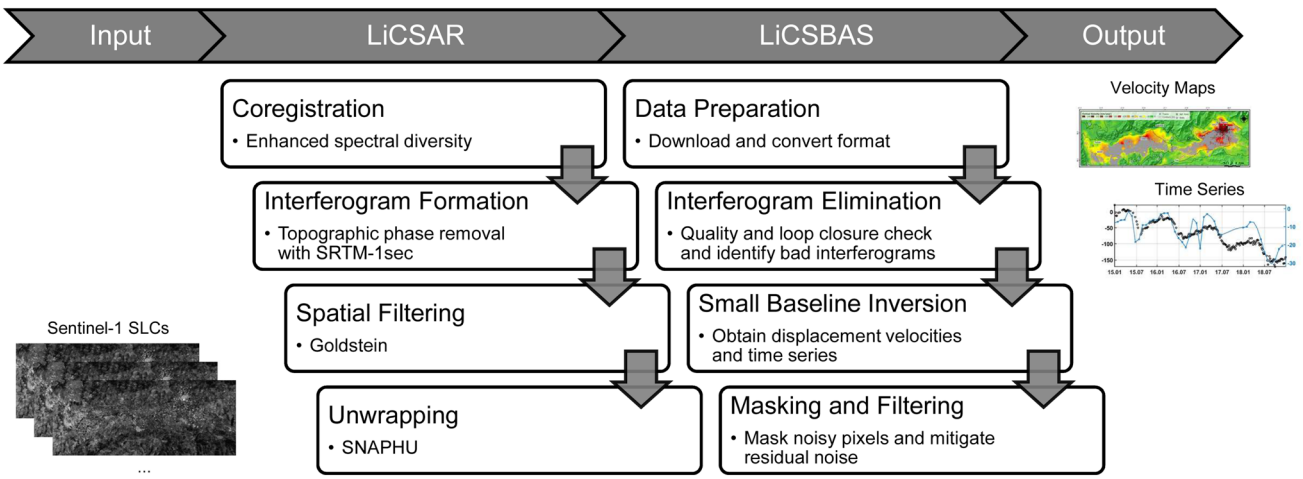

Fig. 4 Main processing steps of LiCSAR and LiCSBAS software tools

used as a reliability measure to mask analysis results, measurement points that show sufficient coherency in both data sets are selected for 3D displacement decomposition. Moreover, acquisition dates of Sentinel-1 products in ascending and descending data sets may not be equally sampled. For that reason, before decomposing the LOS deformation time series into vertical time series, spline interpolation method is applied to both data sets to obtain a common time reference consisting of combined acquisition dates. Spline is often chosen as the interpolation method for InSAR time series, as it can better fit the nonlinear ground displacement processes (Armaş et al. 2017; Bacques et al. 2018; Luo et al. 2020).

Time series decomposition

Like GPS time series, long-term InSAR time series contain components of time-varying seasonal signals and noise in addition to surface displacements of tectonic and non-tectonic origin. Therefore, it is necessary to decompose InSAR time series into several components to analyze the underlying mechanisms more effectively. Both vertical displacement time series and groundwater level data are decomposed into sub-components to better understand short- and long-term patterns and to be able to measure the correlation between them. The general approach is to decompose a time series signal, x, into 3 main additive components as

$$x = x_{\text{trend}} + x_{\text{seas}} + x_{\text{res}}, \quad (1)$$

where x_{trend} is the trend component, x_{seas} is seasonal component and x_{res} denotes the residual component. The additive decomposition approach is used when there is no increase/decrease trend in the magnitude of the seasonal components as time moves on (Hyndman and Athanasopoulos 2018).

One of the classical and relatively simple methods of separating time series into components is called classical decomposition. In the classical decomposition approach, the long-term trend is calculated using a moving average filter. The moving average filter simply smooths data by taking the mean of all adjacent values within a defined filter size. The size of the moving average filter is selected according to the length of seasonality. Afterwards, the detrended signal is obtained by removing the trend from the original signal. And then, each point is averaged in a corresponding year period to estimate the seasonal component. If seasonal filter size is selected long enough, a stable seasonal effect is being produced. Finally, the residual component is calculated by subtracting the estimated trend and the seasonal component.

The filtering approach requires original data to be padded both at the beginning and at the end. Otherwise, there will be no data in decomposed signals since equal-sided filters are used for averaging. The classical approach also tends to smooth rapid changes in the data that could have importance. Such kind of drawbacks triggered the development of more complex algorithms for time series decomposition, such as X11, SEATS, STL (Hyndman and Athanasopoulos 2018). Such kinds of algorithms are more robust to catch rapid changes in trend and do not need additional artificial data at the extremes of time series. However, the classical approach is still widely used since it requires low computational complexity, produces fast results, and allows manual interaction easily (Svetunkov 2022). Besides, it provides successful results as well when data are relatively short and do not have any rapid fluctuations as it is in our case.

In this study, the sampling times of groundwater levels are not equal to the acquisition dates of Sentinel-1. Before starting the decomposing procedure, the groundwater level data are interpolated to the same time reference with vertical displacement time series. The trend filter size is selected to be 61 days as it is the average number of data when both Sentinel-1 A/B are operational. Filter size of 3 is suitable for seasonal average since the magnitude of seasonal change does not have to be the same for all years. The residual signal obtained after the removal of the seasonal and deformation components does not display any systematic signal that can be attributed to ground deformation and hence is not used.

Results

Following the LiCSBAS multi-temporal InSAR processing two main products are obtained; (1) mean velocity maps and (2) displacement time series. Mean velocity maps are compared with geological settings and displacement time series are compared with changes in groundwater levels.

Mean velocity maps

Mean velocity maps in LOS direction are produced for both ascending and descending Sentinel-1 data sets as shown in Fig. 5a, b respectively. The vertical mean deformation velocity map calculated using ascending and descending results is shown in Fig. 5. Since negligible displacements are detected in the E–W direction, they are not used in further analysis. To obtain more reliable pixels, results are masked with coherence threshold (0.05) and other quality criteria like unwrapping errors (Morishita et al. 2020). Warm colors (negative values) from yellow to red represent moving away from the satellite in the LOS direction and highlight subsidence in the vertical direction. It is clear that the entire K. Menderes Graben is subsiding at varying rates from a few cm/year to 24 cm/year. The total area subject to subsidence at a rate of at least 3 cm/year is approximately 688 km^2. Ödemiş town and its surrounding regions are the most severely affected areas with a maximum vertical deformation rate of about 29±0.3 cm/year. While Torbalı and its

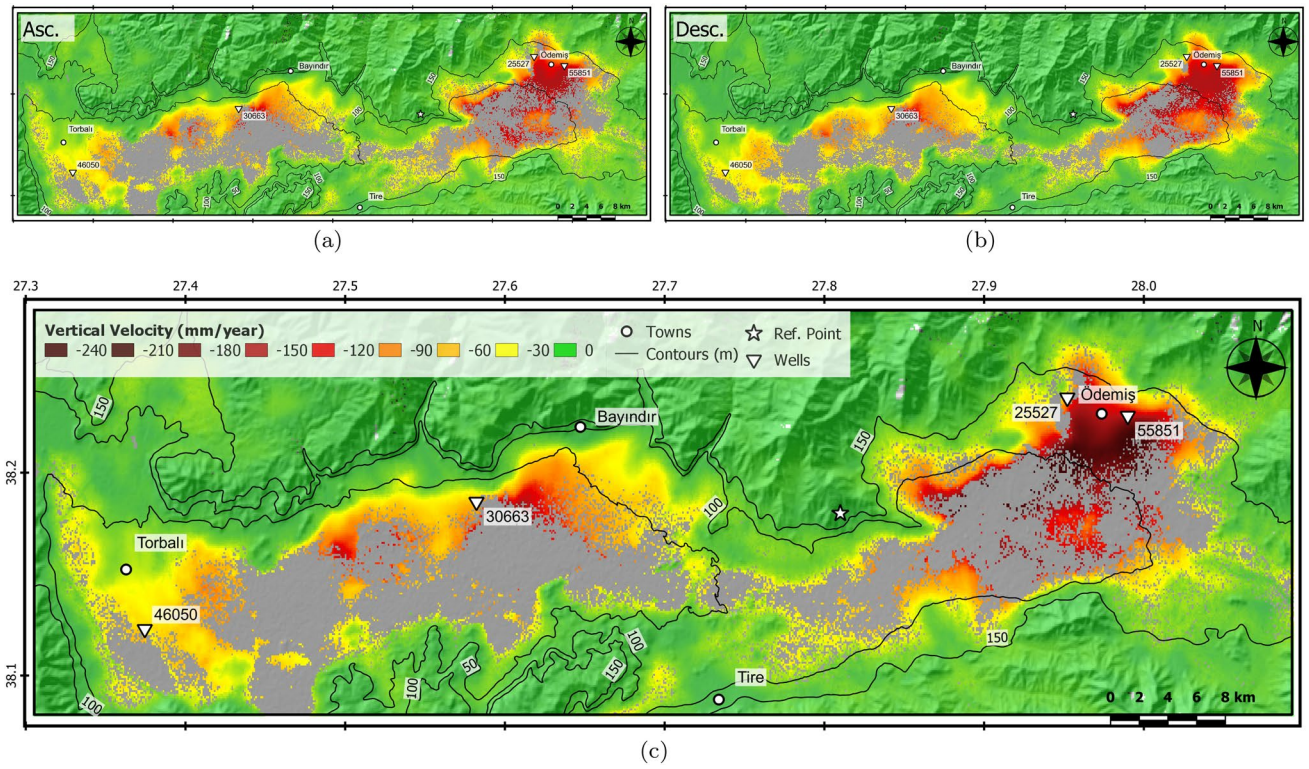

Fig. 5 Mean LOS velocity maps with topographic contours at 50 m intervals (black lines) obtained on ascending track 131 (**a**) and descending track 36 (**b**). **c** Vertical mean velocity map produced by decomposition of the LOS velocities

surroundings and the southern region of Bayındır are also subjected to subsidence, Tire is located in an almost stable region. In general, subsidence increases from east to west and from outside in the basin.

Comparison with geological settings

Figure 6a shows contours lines of the mean vertical velocity field with 3 cm/year intervals on top of a geological map of the K. Menderes Graben (Dubertret and Kalafatcioglu 1973). For a better visualisation, the contours are coloured and created from the unmasked version of the mean vertical velocity field shown in Fig. 5. The K. Menderes Graben is mainly characterized by Quaternary alluvial (Qa) deposits that constitute a relatively flat region from Torbalı to Ödemiş. Alluvial fans, slope debris, and moraines (Qb) are also wide spread in the neighborhood of alluvium deposits. Subsidence is observed mostly in Qa and Qb geological units starting from 3 cm/year in the margins of the graben up to 24 cm/year in the inner part, especially in south of Ödemiş. Thickness off alluvium deposits reaches up to 270 m in the southern of Ödemiş where the most severe subsidence is observed while it decreases towards Bayındır and Torbalı (Rojay et al. 2005). Decreases in the thickness of alluvium deposits and subsidence rates towards the western regions indicate a correlation between the two.

Correlation of geological units and subsidence rates are shown statistically in Fig. 6b. The mean, standard deviation, minimum, and maximum values for each geological unit are calculated. The mean subsidence rates are 3.6 and 2.4 cm/year with standard deviations of ±4.3 and ±3.3 cm/year respectively in Qa and Qb units. The mean and standard deviation of subsidence rate decrease to almost zero in the other units. The maximum subsidence rate is 28.6±0.3 cm/year and observed in Qb units located to the south–southwest of Ödemiş. Statistically, it is clear that there is a very high correlation between the existence of soft sediments, such as alluvium and alluvial fans, and the subsidence rate.

Displacement time series and comparison with groundwater level

Time series of vertical displacements together with groundwater level changes at nearby wells are shown in Fig. 7. In this study, a total of four wells are used to compare displacement time series and groundwater level change: one well in the close vicinity of Bayındır, one well from the south of Torbalı, and two wells around Ödemiş (Fig. 5). The total vertical displacement in 4 years is about 15 cm in Torbalı, 30

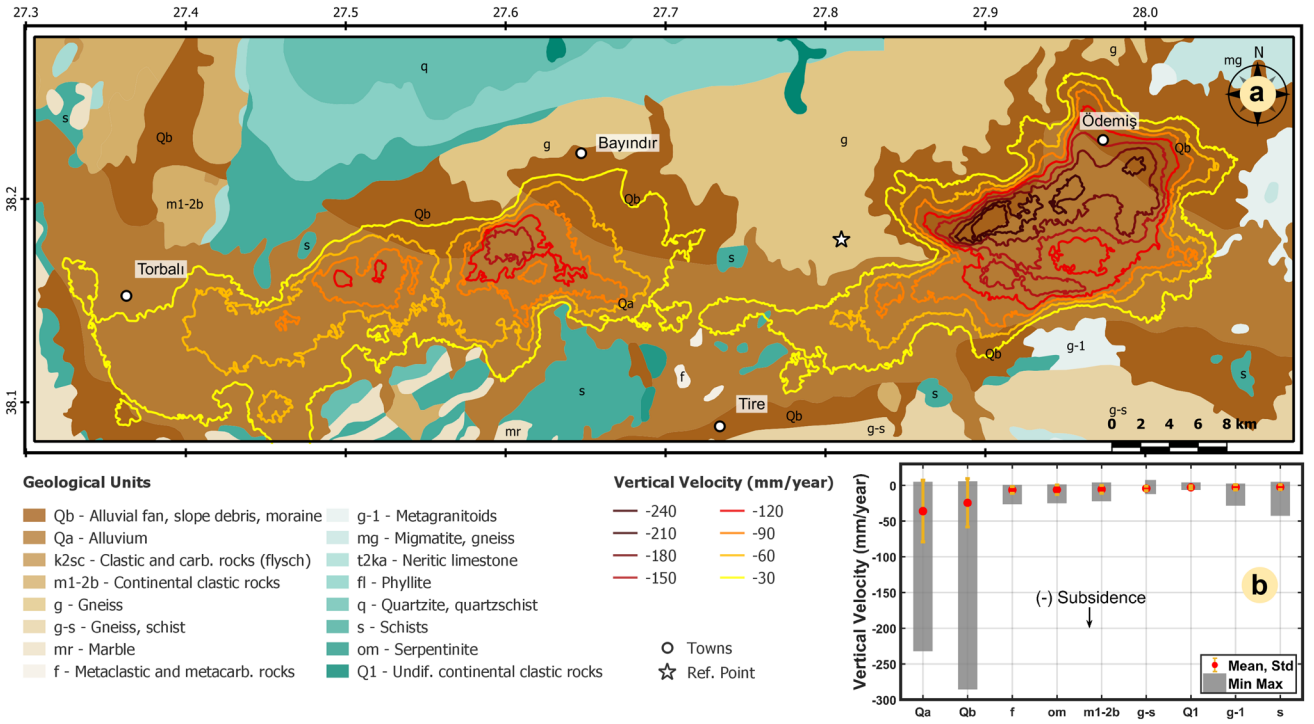

Fig. 6 **a** Geological map of K. Menderes Graben shown together with mean vertical velocity contours at an interval of 3 cm/year. **b** Correlation statistics of geological units and vertical mean deformation velocity. The mean (red dots), standard deviation (orange line), minimum and maximum (bold gray) values of vertical mean velocity are shown for most affected geological units

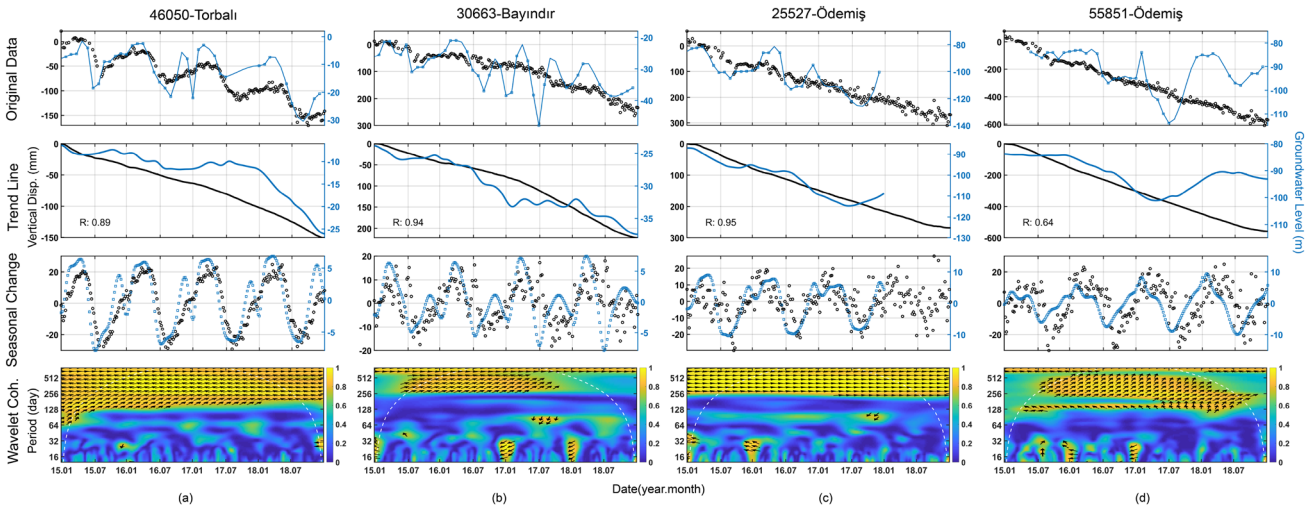

Fig. 7 Time series of groundwater level changes versus subsidence in **a** wells #46050 in Torbalı, **b** #30663 in Bayındır, **c** #25527 in Ödemiş, and **d** #55851 in Ödemiş. Original time series (top raw) are decomposed into trend line (second raw) and seasonal change components (third raw). In the bottom row, seasonal changes are compared using wavelet coherency values

cm in Bayındır, 30 and 60 cm in Ödemiş. The decreases of water levels in these wells during the same period are about 25, 15, 35, and 10 m, respectively. There are some missing values in the water level data (e.g. #25527 in Ödemiş). Water level measurements are also highly irregular. Nevertheless, they demonstrate the positive correlation between decreasing water levels and subsidence. To quantify this relationship, the trend and the seasonal component of both the displacement time series and groundwater levels are calculated and compared.

The classical decomposition method is used to obtain trend and seasonal components for both vertical displacement time series and groundwater levels. Decomposition results are shown for all distinct well locations respectively in Fig. 7a–d. Both displacement time series and groundwater level changes at almost all wells show a general decline trend for all years. The correlation coefficients between trend lines is around 0.9 which is a quite good indication of similarity. The correlation at well #55851 in Ödemiş is the lowest one with an R value of 0.64. In fact, in the first 2.5 years, there seems to be a high correlation. However, groundwater level starts to increase in the last 1.5 years while vertical displacements continue to decrease at the same rate which degrades the correlation.

The seasonal effect in the vertical displacement time series can be observed quite easily even in the original data at well #46050 in Torbalı. In the remaining wells, the periodic effect is visible in the seasonal change component. While the seasonal frequency of displacement time series seems to be more stable, there are many variations in the groundwater levels even within the same seasons. To investigate the seasonal relations of these two time series, wavelet coherence analysis was carried out. Wavelet transformation makes it possible to examine different frequencies (1/period) thoroughly in a time series by decomposing signals into subcomponents with shifted varying frequencies (Daubechies 2009). The cross-correlation between the frequencies in two different time series is calculated by the wavelet coherence method (Torrence and Compo 1998). The wavelet coherency enables the identification of common seasonal patterns between two time series in terms of periodicity and phase. The high coherence values indicate that both signals change in a similar manner within that period. Wavelet coherence graphics in Fig. 7 shows that there is a very high correlation around a period of 1 year. While well #46050 in Torbalı and #25527 in Ödemiş show the same high coherence around 365 days throughout all analysis time, coherence decreases at the last year for other wells. The arrows on the graphs show the phase relations of the time series. The direction of the arrows corresponds to the phase delay in the unit circle. 30° angle of the arrow represents that vertical displacement follows the groundwater level with a delay of approximately 30 days as in the case of wells #46050 and #25527.

Discussion

We observe that the drop in the groundwater level gives rise to subsidence over unconsolidated deposits, a well-known theory first conceptualized by Terzaghi (1925) which states that total stress on the aquifer system is the sum of intergranular stress and pore fluid pressure. Intergranular stress is a simple result of the geological medium and also emphasized as a granular skeleton. Pore pressure is created by groundwater that exists within pore space. The decline in the groundwater level causes a decrease in fluid stress which puts more pressure on the granular skeleton. Increasing stress on the skeleton results in compaction of the medium and ground subsidence occurs.

The strong correlation between the surface subsidence and changes in ground water level observed in the K. Menderes Graben indicates that subsidence results from drop in ground water level which in turn likely result from excessive pumping of ground waters, a conclusion supported by the fact that subsidence is confined only to highly compressible soft alluvial sediments like Qa and Qb. During the 4-year observation period, the entire basin subsides nearly in a linear manner. A seasonal increase of the groundwater induces transient uplift of the ground. However, although the groundwater level increases about 10 m in the last 1.5 years in well #55851, there seems to have been no change in the subsidence trend since then. For this reason, it is necessary to examine in more detail whether the resulting subsidence is irreversible or not.

One way to analyze whether or not a deformation is reversible (recoverable) is to look at the elasticity of the displacement. Ezquerro et al. (2014) and Haghighi and Motagh (2019) proposed to use R value which is simply formulated as a comparison of elastic component vs inelastic component of deformation. The long-term behavior of subsidence is thought to be inelastic deformation since fine-grained soils are consolidated. Due to the observation of continuous subsidence and uplift, periodic short-term changes are considered elastic deformations. Thus, the trend line of the displacement time series reflects inelastic deformation, whereas the seasonal change component gives a sign of elastic deformation. The R value of a single measurement point is then calculated as

$$R = d_{\mathrm{el}}/d_{\mathrm{in}}, \tag{2}$$

where d_{el} is elastic deformation found as the difference of maximum and minimum value in seasonal component and d_{in} is inelastic deformation which is the total amount of displacement observed within a year. To obtain a constant seasonal variation that simplifies our R value calculation for all measurement points, a long seasonal filter size is selected and a R value map is produced as shown in Fig. 8. R values greater than 1 indicate that the elastic response is the dominant component of subsidence, while values lower than 1 indicate that inelastic deformation is dominant. Values close to 0 show strong signs of a high degree of inelastic deformation and irreversible compaction. Although the R value map shows us that inelastic deformation is the dominant component, elastic deformation is also observed in the study area. In general, inelastic deformation highly coexists

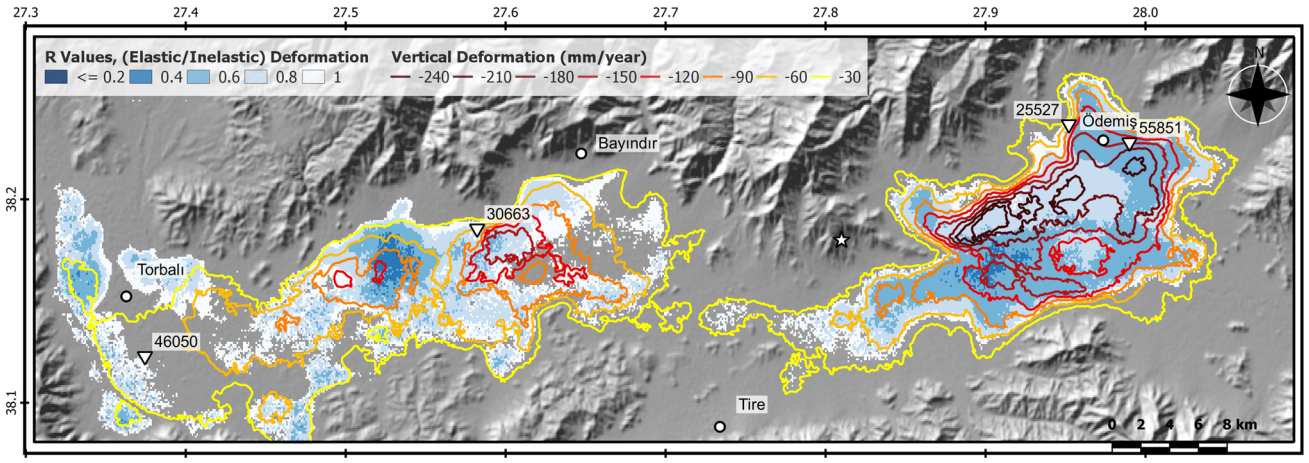

Fig. 8 Color-coded map of R values (d_{el}/d_{in}) on top of SRTM shaded relief image together with contours of subsidence rate at an interval of − 3 cm/year. For the sake of simplicity, only inelastic deformation range is displayed for R values between 0 and 1

together with a high subsidence rate. However, elastic deformation can still exist in some regions where the mean subsidence rate reaches up to 6 cm/year. In some regions, R values around 0.6 could be seen, indicating the high impact of inelastic deformation although the mean subsidence rate is below − 3 cm/year. Thus, a high rate of subsidence does not always mean high inelastic deformation.

Another way of assessing the severity of deformation in the area is to study the relative changes in subsidence and groundwater level changes. Such a comparative attitude may provide more concrete results. This relation is defined as stress–strain analysis which enables us to find the skeletal storage coefficient (compressibility), S_k, in the aquifer system (Riley 1969). S_k is calculated as

$$S_k = \Delta d/\Delta h \tag{3}$$

$$S_k = S_{ke} + S_{kv}, \tag{4}$$

where Δd stands for vertical displacement change and Δh is groundwater level change. Depending on the type of deformation S_k may contain two components, namely the elastic skeletal storage coefficient, S_{ke}, and the inelastic skeletal storage coefficient, S_{kv} (Chen et al. 2016; Rezaei et al. 2020). Then, corresponding vertical displacement difference is changed as elastic, Δd_{el}, or inelastic, Δd_{in}. Groundwater level change during elastic displacement is updated as Δh_{el} and inelastic, Δh_{in}, respectively. While inelastic vertical displacement is identical to the change in the trend line occurred in the long term, elastic displacement is the seasonal max/min value difference in the short term.

Trends of groundwater level changes vary within the analysis period. There is an acceleration in the decreasing trend of well #46050 in Torbalı over the last years. After the drop in groundwater level at well #55851 in Ödemiş ceases in the second half of the analysis period, the ground continues to subside. For that reason, S_{ke} and S_{kv} are calculated annually for all well locations as shown in Table 2. R values are displayed for the entire period since displacement time series show a close linear decrease trend throughout the years. Groundwater wells displayed in Fig. 8 are mostly located in regions of inelastic deformation type with values of R varying below 1. Only well #46050 in Torbalı is within the elastic range with a R value of 1.56. Severe inelastic compression could be around one to two orders greater than elastic compression (Riley 1969; Hoffmann et al. 2001). Well #55851 in Ödemiş shows us the most

Table 2 Inelastic skeletal storage coefficient (S_{kv}), elastic skeletal storage coefficient (S_{ke}), elastic deformation/inelastic deformation ratio (R) for each well

Well	Year	S_{kv}	S_{ke}	R
46050-Torbalı	2015	0.01668	0.00382	1.55808
	2016	0.00722	0.00423	
	2017	0.02185	0.00415	
	2018	0.00337	0.00391	
30663-Bayındır	2015	0.02031	0.00365	0.77739
	2016	0.00515	0.00321	
	2017	0.05900	0.00249	
	2018	0.01328	0.00222	
25527-Ödemiş	2015	0.00819	0.00219	0.84989
	2016	0.00485	0.00234	
	2017	0.01151	0.00281	
	2018	–	–	
55851-Ödemiş	2015	0.47053	0.00613	0.44758
	2016	0.01145	0.00386	
	2017	0.01952	0.00290	
	2018	0.03519	0.00259	

severe inelastic deformation where S_{kv} reaches up to 0.47 value. Although groundwater level is almost steady in 2015 and 2018, subsidence still occurs with a rate of 15 cm/year. It also has the lowest R value of 0.45 which is consistent with S_{kv}. Annual S_{ke} and S_{kv} values are unstable since there is no steady decrease in the groundwater level. All wells, including #46050 in Torbalı, have greater S_{kv} values for almost all years. However, the differences between S_{ke} and S_{kv} for the well #46050 in Torbalı are much less than those in other wells. even in 2018 the value of S_{ke} is greater than S_{kv}. Therefore, inelastic/elastic skeletal storage coefficient values support the outputs of R value analysis. For lower R values which indicate dominant inelastic deformation, S_{kv} is much greater than S_{ke}.

Conclusion

Ground surface deformations previously observed in the K. Menderes Graben are analyzed by multi-temporal InSAR techniques using Sentinel-1 SAR data acquired in 2015–2018. The main results of the analysis can be summarized as follows;

- Almost the entire graben is subsiding at rates reaching as much ash 29 cm/year, making it one of the fastest subsiding regions in the world.
- Ground displacement is spatially correlated with the distribution of unconsolidated sediments, such as alluvial deposits, slope debris, and moraines.
- There is also a strong temporal correlation between groundwater-level changes and subsidence.
- Aforementioned observations suggest that subsidence is the direct result of groundwater level changes.

We also examine whether the observed deformation is inelastic or elastic. Obtained results regarding this issue are:

- R value calculations indicate that inelastic deformation is the dominant component in most parts of the region. This is an indication of irreversible deformation taking place in the region.
- Skeletal storage coefficients, S_{ke} and S_{kv}, in the corresponding well locations also support the idea of inelastic deformation.

However, severe inelastic deformation is not extensive, and the region may still recover from the deformation phenomenon. Groundwater management of the K. Menderes basin such as artificial refill methods as explained in Peksezer (2010) and Sayit and Yazicigil (2012)), can cease the severity of subsidence and even cause uplift. Similar control strategies to mitigate the effect of subsidence due to overexploitation of groundwater seem to be quite effective in different regions of the world like Las Vegas valley in Nevada (Bell et al. 2008), Madrid aquifer (Ezquerro et al. 2014), Santa Clara valley in California (Chaussard et al. 2017), Shanghai City (He et al. 2019), Querétaro Valley in central Mexico (Tang et al. 2022), and Taiyuan basin in Northern China (Tang et al. 2022)

As a future work, it is crucial to construct a deformation model to better understand the current deformation process in the region and to predict future behavior. Interpretation of the deformation process and its spatio-temporal relation to groundwater levels changes and geological units would become more concrete with numerical/mathematical models (Shen and Xu 2011; Shen et al. 2013; Xu et al. 2015; Guzy and Malinowska 2020).

Acknowledgements This is a part of the Ph.D. dissertation of Mümin Imamoglu. We thank you for using the facilities of TUBITAK BİLGEM and Yıldız Technical University, and also we thank the Republic of Turkey Ministry of Interior Disaster and Emergency Management Presidency (AFAD) for providing the active faults and geological settings maps of the study region.

Funding No funding was received to assist with the preparation of this manuscript.

Availability of data and material Not applicable.

Declarations

Conflict of interest The authors declare that they have no conflict of interest.

Code availability Not applicable.

References

Armaş I, Mendes DA, Popa RG, Gheorghe M, Popovici D (2017) Long-term ground deformation patterns of Bucharest using multitemporal InSAR and multivariate dynamic analyses: a possible transpressional system? Sci Rep 7(1):1–13

Aslan G, Cakir Z, Lasserre C, Renard F (2019) Investigating subsidence in the bursa plain, Turkey, using ascending and descending Sentinel-1 satellite data. Remote Sens 11(1):85

Aslan G, Foumelis M, Raucoules D, De Michele M, Bernardie S, Cakir Z (2020) Landslide mapping and monitoring using persistent scatterer interferometry (psi) technique in the French alps. Remote Sens 12(8):1305

Bacques G, de Michele M, Raucoules D, Aochi H, Rolandone F (2018) Shallow deformation of the San Andreas fault 5 years following the 2004 Parkfield earthquake (Mw6) combining ERS2 and Envisat InSAR. Sci Rep 8(1):1–10

Bekaert DP, Handwerger AL, Agram P, Kirschbaum DB (2020) InSAR-based detection method for mapping and monitoring slow-moving landslides in remote regions with steep and mountainous terrain: an application to nepal. Remote Sens Environ 249:111983

Bell JW, Amelung F, Ferretti A, Bianchi M, Novali F (2008) Permanent scatterer InSAR reveals seasonal and long-term aquifer-system

response to groundwater pumping and artificial recharge. Water Resour Res 44(2)
Berardino P, Fornaro G, Lanari R, Sansosti E (2002) A new algorithm for surface deformation monitoring based on small baseline differential SAR interferograms. IEEE Trans Geosci Remote Sens 40(11):2375–2383
Besoya M, Govil H, Bhaumik P (2021) A review on surface deformation evaluation using multitemporal SAR interferometry techniques. Spatial Information Research 29(3):267–280. https://doi.org/10.1007/s41324-020-00344-8
Biggs J, Wright TJ (2020) How satellite InSAR has grown from opportunistic science to routine monitoring over the last decade. Nat Commun 11(1):1–4
Bletery Q, Cavalié O, Nocquet JM, Ragon T (2020) Distribution of interseismic coupling along the north and east anatolian faults inferred from InSAR and GPS data. Geophys Res Lett 47(16):e2020GL087775
Chang L, Ku O, Hanssen RF (2019) Identification of deformation pattern changes caused by enhanced oil recovery (EOR) using InSAR. Int J Remote Sens 40(4):1495–1505
Chaussard E, Milillo P, Bürgmann R, Perissin D, Fielding EJ, Baker B (2017) Remote sensing of ground deformation for monitoring groundwater management practices: application to the Santa Clara valley during the 2012–2015, California drought. J Geophys Res Solid Earth 122(10):8566–8582
Chen CW, Zebker HA (2002) Phase unwrapping for large SAR interferograms: statistical segmentation and generalized network models. IEEE Trans Geosci Remote Sens 40(8):1709–1719
Chen J, Knight R, Zebker HA, Schreüder WA (2016) Confined aquifer head measurements and storage properties in the san Luis valley, Colorado, from spaceborne InSAR observations. Water Resour Res 52(5):3623–3636
Crosetto M, Monserrat O, Cuevas-González M, Devanthéry N, Crippa B (2016) Persistent scatterer interferometry: a review. ISPRS J Photogramm Remote Sens 115:78–89
Crosetto M, Solari L, Balasis-Levinsen J, Casagli N, Frei M, Oyen A, Moldestad D (2020) Ground deformation monitoring at continental scale: the European ground motion service. Int Arch Photogramm Remote Sens Spat Inf Sci 43:293–298
D'Amico F, Gagliardi V, Ciampoli LB, Tosti F (2020) Integration of InSAR and GPR techniques for monitoring transition areas in railway bridges. NDT E Int 115:102291
Daubechies I (2009) The wavelet transform, time-frequency localization and signal analysis. Princeton University Press, Princeton
De Luca C, Zinno I, Manunta M, Lanari R, Casu F (2017) Large areas surface deformation analysis through a cloud computing p-sbas approach for massive processing of dInSAR time series. Remote Sens Environ 202:3–17
Dehls JF, Larsen Y, Marinkovic P, Lauknes TR, Stødle D, Moldestad DA (2019) InSAR. no: A national InSAR deformation mapping/monitoring service in Norway-from concept to operations. In: IGARSS 2019-2019 IEEE international geoscience and remote sensing symposium. IEEE, pp 5461–5464
Demirtaş R, Yaman M, Tepeuğur E (2002) Ödemiş'de Yüzeyde Oluşan Deformasyonların Oluşum Mekanizması. https://www.academia.edu/8775970/. Accessed 04 Jan 2021
Demirtaş R, Ercan S, Demir B, Aktan M (2021) Ege Çöküntü Alanında Son 20 Yıl Süresince Oluşmuş ve Oluşmaya Devam Eden Yüzey Deformasyonları Deprembilimcilere Ne Söylemeye Çalışıyor? https://www.academia.edu/8775613/. Accessed 04 Jan 2021
Dubertret L, Kalafatcioglu A (1973) 1:500000 ölçekli Türkiye Jeolojik Harita ve izahnamesi-izmir Paftası. MTA Yayınl
Dumont JF, Uysal ŞŞŞ, Karamanderesi IH, Letouzey J (1979) Formation of the grabens in southwestern anatolia. Maden Tetkik ve Arama Dergisi 92(92):7–18
Elliott J, de Michele M, Gupta H (2020) Earth observation for crustal tectonics and earthquake hazards. Surv Geophys 41(6):1355–1389
Emil MK, Sultan M, Alakhras K, Sataer G, Gozi S, Al-Marri M, Gebremichael E (2021) Countrywide monitoring of ground deformation using InSAR time series: a case study from qatar. Remote Sens 13(4):702
Emre Ö, Duman TY, Özalp S, Şaroğlu F, Olgun Ş, Elmacı H, Can T (2018) Active fault database of turkey. Bull Earthq Eng 16(8):3229–3275
Eris E, Cavus Y, Aksoy H, Burgan HI, Aksu H, Boyacioglu H (2020) Spatiotemporal analysis of meteorological drought over kucuk menderes river basin in the Aegean region of turkey. Theor Appl Climatol 142(3):1515–1530
Ezquerro P, Herrera G, Marchamalo M, Tomás R, Béjar-Pizarro M, Martínez R (2014) A quasi-elastic aquifer deformational behavior: Madrid aquifer case study. J Hydrol 519:1192–1204
Fadhillah MF, Achmad AR, Lee CW (2020) Integration of InSAR time-series data and GIS to assess land subsidence along subway lines in the Seoul metropolitan area. South Korea. Remote Sens 12(21):3505
Fan H, Wang L, Wen B, Du S (2021) A new model for three-dimensional deformation extraction with single-track InSAR based on mining subsidence characteristics. Int J Appl Earth Obs Geoinf 94:102223
Farr TG, Rosen PA, Caro E, Crippen R, Duren R, Hensley S, Kobrick M, Paller M, Rodriguez E, Roth L et al (2007) The shuttle radar topography mission. Rev Geophys 45(2)
Ferretti A, Prati C, Rocca F (2001) Permanent scatterers in SAR interferometry. IEEE Trans Geosci Remote Sens 39(1):8–20
Gee D, Sowter A, Grebby S, de Lange G, Athab A, Marsh S (2019) National geohazards mapping in Europe: interferometric analysis of the Netherlands. Eng Geol 256:1–22
Gheorghe M, Armaş I, Dumitru P, Călin A, Bădescu O, Necsoiu M (2020) Monitoring subway construction using Sentinel-1 data: a case study in Bucharest, Romania. Int J Remote Sens 41(7):2644–2663
Goldstein RM, Werner CL (1998) Radar interferogram filtering for geophysical applications. Geophys Res Lett 25(21):4035–4038
Gülersoy AE, Çelik MA (2015) Determining of areas with high erosion risk in küçük menderes river basin (west anatolia, turkey) by using multi-criteria decision making method. Fresenius Environ Bull 24(1a):195–202
Guzy A, Malinowska AA (2020) State of the art and recent advancements in the modelling of land subsidence induced by groundwater withdrawal. Water 12(7):2051
Haghighi MH, Motagh M (2019) Ground surface response to continuous compaction of aquifer system in Tehran, Iran: results from a long-term multi-sensor InSAR analysis. Remote Sens Environ 221:534–550
Halicioglu K, Erten E, Rossi C (2021) Monitoring deformations of Istanbul metro line stations through Sentinel-1 and levelling observations. Environ Earth Sci 80(9):1–10
Hanssen R, Usai S (1997) Interferometric phase analysis for monitoring slow deformation processes. ESA SP (Print) pp 487–491
He XC, Yang TL, Shen SL, Xu YS, Arulrajah A (2019) Land subsidence control zone and policy for the environmental protection of Shanghai. Int J Environ Res Public Health 16(15):2729
Herrera-García G, Ezquerro P, Tomás R, Béjar-Pizarro M, López-Vinielles J, Rossi M, Mateos RM, Carreón-Freyre D, Lambert J, Teatini P et al (2021) Mapping the global threat of land subsidence. Science 371(6524):34–36
Hoffmann J, Zebker HA, Galloway DL, Amelung F (2001) Seasonal subsidence and rebound in las Vegas Valley, Nevada, observed by synthetic aperture radar interferometry. Water Resour Res 37(6):1551–1566

Hooper A, Bekaert D, Spaans K, Arıkan M (2012) Recent advances in SAR interferometry time series analysis for measuring crustal deformation. Tectonophysics 514:1–13
Hu J, Li Z, Ding X, Zhu J, Zhang L, Sun Q (2014) Resolving three-dimensional surface displacements from InSAR measurements: a review. Earth Sci Rev 133:1–17
Hu J, Ding X, Li Z, Zhang L, Zhu J, Sun Q, Gao G (2016) Vertical and horizontal displacements of Los angeles from InSAR and GPS time series analysis: resolving tectonic and anthropogenic motions. J Geodyn 99:27–38
Hyndman RJ, Athanasopoulos G (2018) Forecasting: principles and practice. OTexts
Imamoglu M, Kahraman F, Cakir Z, Sanli FB (2019) Ground deformation analysis of bolvadin (w turkey) by means of multitemporal InSAR techniques and Sentinel-1 data. Remote Sens 11(9):1069
Izmir V (2019) Nehir havza yönetim planı nihai raporu. Tech. rep., T.C. İzmir Valiliği Çevre Ve Şehircilik İl Müdürlüğü
Kalia A, Frei M, Lege T (2017) A copernicus downstream-service for the nationwide monitoring of surface displacements in Germany. Remote Sens Environ 202:234–249
Klees R, Massonnet D (1998) Deformation measurements using SAR interferometry: potential and limitations. Geol Mijnb 77(2):161–176
KOERI (2021) B.U. KOERI-RETMC Earthquake Catalogue. Boğaziçi University Kandilli Observatory and Earthquake Research Institute Regional Earthquake-Tsunami Monitoring Center. http://www.koeri.boun.edu.tr/sismo/2/earthquake-catalog/. Accessed 04 Jan 2021
Lanari R, Bonano M, Casu F, Luca CD, Manunta M, Manzo M, Onorato G, Zinno I (2020) Automatic generation of Sentinel-1 continental scale dInSAR deformation time series through an extended p-sbas processing pipeline in a cloud computing environment. Remote Sens 12(18):2961
Lanari R, Reale D, Bonano M, Verde S, Muhammad Y, Fornaro G, Casu F, Manunta M (2020) Comment on "pre-collapse space geodetic observations of critical infrastructure: the morandi bridge genoa Italy" by milillo et al. (2019). Remote Sens 12(24):4011
Lauknes T, Shanker AP, Dehls J, Zebker H, Henderson I, Larsen Y (2010) Detailed rockslide mapping in Northern Norway with small baseline and persistent scatterer interferometric SAR time series methods. Remote Sens Environ 114(9):2097–2109
Lazeckỳ M, Spaans K, González PJ, Maghsoudi Y, Morishita Y, Albino F, Elliott J, Greenall N, Hatton E, Hooper A et al (2020) LiCSAR: an automatic InSAR tool for measuring and monitoring tectonic and volcanic activity. Remote Sens 12(15):2430
LiCSAR (2021) COMET-LiCS Sentinel-1 InSAR Portal. Available online. https://comet.nerc.ac.uk/COMET-LiCS-portal/. Accessed 04 Jan 2021
Luo X, Wang C, Long Y, Yi Z (2020) Analysis of the decadal kinematic characteristics of the Daguangbao landslide using multiplatform time series InSAR observations after the Wenchuan earthquake. J Geophys Res Solid Earth 125(12):e2019JB019325
Morishita Y (2021) Nationwide urban ground deformation monitoring in japan using Sentinel-1 LiCSAR products and LiCSBAS. Prog Earth Planet Sci 8(1):1–23
Morishita Y, Lazecky M, Wright TJ, Weiss JR, Elliott JR, Hooper A (2020) LiCSBAS: an open-source InSAR time series analysis package integrated with the LiCSAR automated Sentinel-1 InSAR processor. Remote Sens 12(3):424
Osmanoğlu B, Sunar F, Wdowinski S, Cabral-Cano E (2016) Time series analysis of InSAR data: methods and trends. ISPRS J Photogramm Remote Sens 115:90–102
Ozkaymak C, Sozbilir H, Gecievi MO, Tiryakioglu I (2019) Late holocene coseismic rupture and aseismic creep on the bolvadin fault, afyon akşehir graben, western anatolia. Turk J Earth Sci 28(6):787–804
Peksezer A (2010) Artificial recharge of groundwater in küçük menderes river basin, turkey. Master's thesis, METU
Pepe A, Calò F (2017) A review of interferometric synthetic aperture radar (InSAR) multi-track approaches for the retrieval of earth's surface displacements. Appl Sci 7(12):1264
Poyraz F, Hastaoğlu KÖ (2020) Monitoring of tectonic movements of the gediz graben by the psInSAR method and validation with GNSS results. Arab J Geosci 13(17):1–11
Pusatli OT, Camur MZ, Yazicigil H (2009) Susceptibility indexing method for irrigation water management planning: applications to k Menderes river basin, Turkey. J Environ Manag 90(1):341–347
Rezaei A, Mousavi Z, Khorrami F, Nankali H (2020) Inelastic and elastic storage properties and daily hydraulic head estimates from continuous global positioning system (GPS) measurements in northern Iran. Hydrogeol J 28(2):657–672
Riley FS (1969) Analysis of borehole extensometer data from central California. Land Subsid 2:423–431
Rojay B, Toprak V, Demirci C, Süzen L (2005) Plio-quaternary evolution of the küçük menderes graben southwestern anatolia, turkey. Geodin Acta 18(3–4):317–331
Şahin Y, Alper B, Tayfur G (2018) Küçük menderes havzası su kaynaklarının sürdürülebilirliği. DÜMF Mühendislik Dergisi 9(2):955–962
Sayit AP, Yazicigil H (2012) Assessment of artificial aquifer recharge potential in the kucuk menderes river basin, turkey. Hydrogeol J 20(4):755–766
Selvakumaran S (2020) Interferometric synthetic aperture radar for remote satellite monitoring of bridges. Ph.D. thesis, University of Cambridge
Shen SL, Xu YS (2011) Numerical evaluation of land subsidence induced by groundwater pumping in shanghai. Can Geotech J 48(9):1378–1392
Shen SL, Ma L, Xu YS, Yin ZY (2013) Interpretation of increased deformation rate in aquifer iv due to groundwater pumping in shanghai. Can Geotech J 50(11):1129–1142
Solari L, Del Soldato M, Raspini F, Barra A, Bianchini S, Confuorto P, Casagli N, Crosetto M (2020) Review of satellite interferometry for landslide detection in italy. Remote Sens 12(8):1351
Staniewicz S, Chen J, Lee H, Olson J, Savvaidis A, Reedy R, Breton C, Rathje E, Hennings P (2020) InSAR reveals complex surface deformation patterns over an 80,000 km^2 oil-producing region in the Permian basin. Geophys Res Lett 47(21):e2020GL090151
Svetunkov I (2022) Forecasting and analytics with ADAM. https://openforecast.org/adam/. Accessed 08 Feb 2022
Tang W, Zhao X, Motagh M, Bi G, Li J, Chen M, Chen H, Liao M (2022) Land subsidence and rebound in the Taiyuan basin, northern China, in the context of inter-basin water transfer and groundwater management. Remote Sens Environ 269:112792
Terzaghi K (1925) Principles of soil mechanics, iv-settlement and consolidation of clay. Eng News Rec 95(3):874–878
TOB (2018) İzmir İli 2018 yılı Çevre durum raporu. Tech. rep., T.C. Tarım ve Orman Bakanlığı Su Yönetimi Genel Müdürlüğü
Torrence C, Compo GP (1998) A practical guide to wavelet analysis. Bull Am Meteorol Soc 79(1):61–78
Torres R, Snoeij P, Geudtner D, Bibby D, Davidson M, Attema E, Potin P, Rommen B, Floury N, Brown M et al (2012) Gmes Sentinel-1 mission. Remote Sens Environ 120:9–24
Weiss JR, Walters RJ, Morishita Y, Wright TJ, Lazecky M, Wang H, Hussain E, Hooper AJ, Elliott JR, Rollins C et al (2020) High-resolution surface velocities and strain for anatolia from Sentinel-1 InSAR and GNSS data. Geophys Res Lett 47(17):e2020GL087376

Xu YS, Yuan Y, Shen SL, Yin ZY, Wu HN, Ma L (2015) Investigation into subsidence hazards due to groundwater pumping from aquifer II in Changzhou, China. Nat Hazards 78(1):281–296

Xu X, Zhao D, Ma C, Lian D (2020) Monitoring subsidence deformation of suzhou subway using InSAR timeseries analysis. IEEE Access

Yagbasan O (2016) Impacts of climate change on groundwater recharge in küçük menderes river basin in western turkey. Geodin Acta 28(3):209–222

Yang Z, Li Z, Zhu J, Wang Y, Wu L (2020) Use of SAR/InSAR in mining deformation monitoring, parameter inversion, and forward predictions: a review. IEEE Geosci Remote Sens Mag 8(1):71–90